Golgi fragmentation in *pmn* mice is due to a defective ARF1/TBCE cross-talk that coordinates COPI vesicle formation and tubulin polymerization

Sarah Bellouze[1], Michael K Schäfer[2], Dorothée Buttigieg[1], Gilbert Baillat[1], Catherine Rabouille[3,4] and Georg Haase[1,*

[1]Institut de Neurosciences de la Timone, Centre National de la Recherche Scientifique (CNRS) and Aix-Marseille Université UMR7289, Marseille, France, [2]Klinik für Anästhesiologie, Universitätsmedizin Mainz, Mainz, Germany, [3]Hubrecht Institute-KNAW and [4]Department of Cell Biology, University Medical Center Utrecht, Utrecht, The Netherlands

Golgi fragmentation is an early hallmark of many neurodegenerative diseases but its pathophysiological relevance and molecular mechanisms are unclear. We here demonstrate severe and progressive Golgi fragmentation in motor neurons of progressive motor neuronopathy *(pmn)* mice due to loss of the Golgi-localized tubulin-binding cofactor E (TBCE). Loss of TBCE in mutant *pmn* and TBCE-depleted motor neuron cultures causes defects in Golgi-derived microtubules, as expected, but surprisingly also reduced levels of COPI subunits, decreased recruitment of tethering factors p115/GM130 and impaired Golgi SNARE-mediated vesicle fusion. Conversely, ARF1, which stimulates COPI vesicle formation, enhances the recruitment of TBCE to the Golgi, increases polymerization of Golgi-derived microtubules and rescues TBCE-linked Golgi fragmentation. These data indicate an ARF1/TBCE-mediated cross-talk that coordinates COPI formation and tubulin polymerization at the Golgi. We conclude that interruption of this cross-talk causes Golgi fragmentation in *pmn* mice and hypothesize that similar mechanisms operate in human amyotrophic lateral sclerosis and spinal muscular atrophy.

INTRODUCTION

The mammalian Golgi apparatus is a single copy membrane-bound organelle that comprises stacked flattened cisternae. It lays at the heart of the secretory pathway where it controls the processing and dispatching of proteins *en route* from their site of synthesis in the endoplasmic reticulum to their final subcellular destination (1). Remarkably, structural and functional alterations of the Golgi apparatus are a common hallmark of many neurodegenerative diseases including Parkinson, Alzheimer and prion disease (2). They are best characterized in amyotrophic lateral sclerosis (ALS) where Golgi fragmentation and atrophy are among the earliest pathological features of degenerating motor neurons (3,4).

Two main hypotheses have been proposed to explain pathological Golgi fragmentation in ALS. The first hypothesis focuses on microtubule defects. Indeed, Golgi fragmentation observed in degenerating motor neurons of transgenic mutant SOD1 mice (4), the most widely used familial ALS model,

bears similarities with the change in the Golgi organization induced by microtubule-depolymerizing agents in cell culture (5–7). In addition, the microtubule-destabilizing protein Stathmin is strongly up-regulated in the spinal cord of these mice (8). The second hypothesis incriminates protein misfolding or mislocalization. Aggregation-prone mutant SOD1 proteins have been shown to mislocalize in the lumen of the Golgi apparatus (9) but see (10), to inhibit anterograde protein transport and to cause Golgi fragmentation *in vitro* (11,12).

To investigate whether microtubule defects or protein misfolding/mislocalization are the primary cause of Golgi fragmentation in degenerating motor neurons *in vivo*, we took advantage of the unique features of *progressive motor neuronopathy* (*pmn*) mice (13). These mice bear a mutation in the tubulin-binding cofactor E (TBCE) gene (14,15) which encodes one of at least five tubulin-specific chaperones (TBCA–TBCE) known to promote tubulin folding and microtubule polymerization (16,17). TBCE is prominently expressed in motor neurons (14) where it localizes to the Golgi and shuttles as a peripheral membrane-associated protein

*To whom correspondence should be addressed at: Institut de Neurosciences de la Timone, UMR 7289 CNRS Aix-Marseille University 27, boulevard Jean Moulin, 13385 Marseille cx 5, France. Tel: +33 673238113; Fax: +33 491324056; Email: georg.haase@univ-amu.fr

between the Golgi membrane and the cytosol (18). The importance of TBCE function in human disease is underscored by autosomal recessive TBCE mutations in patients with Sanjad–Sakati/Kenny–Caffey syndrome suffering from severe growth and mental retardation, facial dysmorphism and congenital hypoparathyroidism (19).

The *pmn* mutation, a homozygous Trp–Gly exchange at the C-terminus of TBCE, destabilizes the protein (14) which decreases the level of polymerized microtubules but increases the level of soluble tubulin (18), allowing to test the two above mentioned hypotheses on the molecular mechanism of Golgi fragmentation. Furthermore, microtubule loss in *pmn* mice starts in distal axons leading to axonal dying back (18) but leaves motor neuron cell bodies in spinal cord intact (20) enabling to investigate Golgi structure during the entire disease course.

Here, we show that in *pmn* mice as in human ALS, Golgi fragmentation is one of the earliest features of degenerating motor neurons. Loss of TBCE in *pmn* spinal motor neurons and in TBCE-depleted NSC34 motor neuron cultures impairs the polymerization of Golgi-derived microtubules, as expected, but surprisingly also results in the loss of COPI vesicle subunits, defective localization of Golgi tethering factors and increased levels of ER-Golgi v-SNAREs, yet impaired SNARE pair formation, all features sustaining the observed changes in Golgi architecture and leading to extensive Golgi vesiculation. Conversely, ARF1 that drives COPI vesicle formation recruits TBCE to the Golgi membrane, enhances polymerization of Golgi-derived microtubules and rescues TBCE-linked Golgi fragmentation. These data unravel an unprecedented ARF1/TBCE-mediated cross-talk that coordinates COPI formation and tubulin polymerization at the Golgi. We conclude that defective TBCE function in the cross-talk causes Golgi fragmentation in *pmn* motor neurons and hypothesize that similar mechanisms operate in other motor neuron diseases such as SOD1-linked ALS and SMA.

RESULTS

Golgi fragmentation and atrophy in *pmn* motor neurons involves severe progressive Golgi vesiculation

To investigate whether Golgi structure is altered in motor neurons of *pmn* mice, we first used a microscopy approach. When examined in lumbar spinal cord cryosections of 25-day-old mice by immunofluorescence for the Golgi transmembrane protein MG160, the Golgi of *pmn* motor neurons is fragmented and atrophied when compared with wild-type littermates (Fig. 1A–E and Supplementary Material, Fig. S1A–B), whereas ER (KDEL) and early endosomes (EEA1) appear normal (Supplementary Material, Fig. S1C–D).

When examined by electron microscopy, the Golgi in the cell body of wild-type motor neurons exhibits the typical morphology of stacked cisternae (Fig. 1F). In *pmn* motor neurons, however, three prominent types of Golgi alterations are observed (Fig. 1F). In the first, some Golgi cisternae are disrupted and replaced by tubules and vesicles whereas others remain intact ('partially vesicular'). In the second, Golgi cisternae are completely transformed into dense clusters of numerous tubules and small vesicles of ∼40–50 nm in diameter ('completely

vesicular'). In the third, only small remnants of fragmented Golgi are observed ('remnant'). Between Day 15 when the first symptoms appear and Day 35 just before the animal's death, the frequency of completely vesiculated Golgi increases four fold (Fig. 1G), suggesting that Golgi fragmentation and atrophy in *pmn* motor neurons is due to progressive Golgi vesiculation.

Loss of TBCE results in COPI degradation and dispersion of the tethers p115/GM130

To start addressing the mechanisms of Golgi vesiculation in *pmn* motor neurons, we asked whether the formation and trafficking of COPI, COPII and clathrin-coated vesicles that mediate transport to, through and from the Golgi (1) is affected. To do so, we assessed the expression of specific coat proteins. The immunoreactivity of the COPI coat subunit β-COP is almost undetectable in *pmn* motor neurons (Fig. 2A) and the protein levels of β-COP and ε-COP in *pmn* spinal cords are strongly reduced when assessed by western blot (Fig. 2B), whereas the levels of clathrin, the COPII coat subunit Sec23 and also the intraluminal Golgi-resident enzymes Mannosidase II (MannII) and Galactosyltransferase (GalT) are similar in *pmn* and wild-type tissues (Fig. 2B). To investigate this further, we used NSC34 motor neuron cultures where endogenous TBCE was completely depleted (Fig. 2C–E). Similar to *pmn* motor neurons *in vivo*, TBCE-depleted NSC34 cells exhibit extensive Golgi fragmentation observed by the pattern of MannII-green fluorescent protein (GFP) (Fig. 2C), as well as strongly decreased β-COP levels observed by immunofluorescence (Fig. 2C), western blot (Fig. 2D) and flow cytometry (Fig. 2E).

Since β-COP directly interacts with a number of vesicle tethering proteins including p115 (22), we then tested whether the reduction of β-COP impacts on p115 and indirectly on GM130, a known p115 interactor (23). p115 and GM130 show reduced immunofluorescence signals at the Golgi of *pmn* motor neurons (Fig. 2F) but unaltered protein levels in *pmn* spinal cords (Fig. 2G), suggesting that the loss of the COPI coat affects the membrane recruitment of these tethering proteins but not their stability. Cell fractionation (Fig. 2H) confirmed that a significant pool of p115 and GM130 is cytosolic in *pmn* spinal cord contrasting with their exclusive association with membranes in wild-type. Similarly, TBCE-depleted motor neurons in culture display more hazy GM130 immunofluorescence (Fig. 2I) and decreased membrane-bound p115 (Fig. 2J).

To characterize these changes quantitatively, we fractionated cell compartments on sucrose gradients (Fig. 2K). In control cells, TBCE, MannII and GM130 are confined to light fractions containing Golgi membranes whereas β-COP is expressed in membranes of increasing densities, including fractions of 1.14–1.36 M sucrose known to contain COPI vesicles (21). Conversely, in TBCE-depleted cells, β-COP expression is specifically lost in the vesicle fractions and GM130 is no longer associated to Golgi membrane (Fig. 2K), confirming that loss of TBCE function leads to β-COP redistribution and degradation as well as reduced membrane recruitment of tethers. Since β-COP degradation is sufficient to cause vesicle accumulation and GM130 redistribution in HeLa cells (24), it most likely
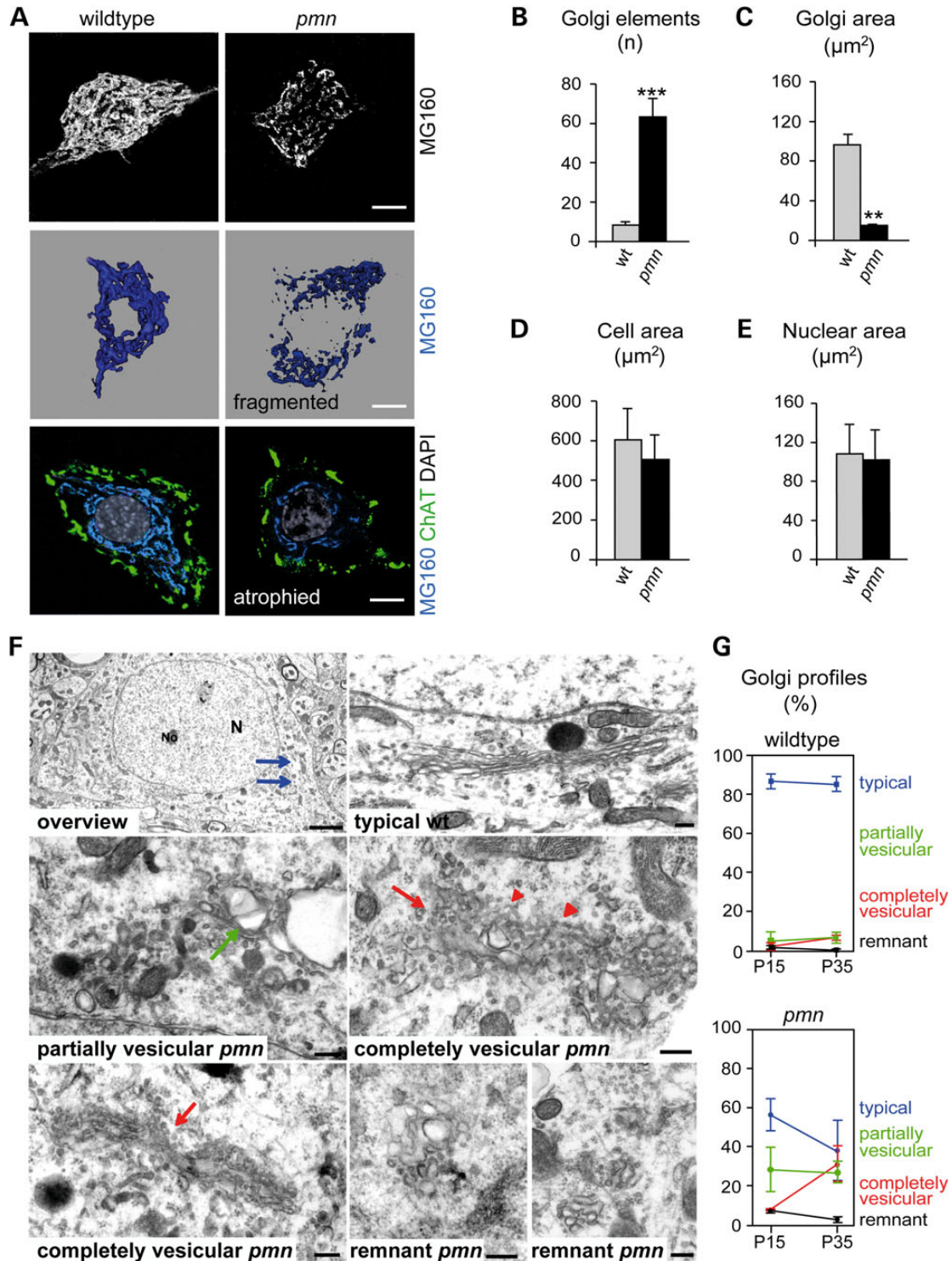
Figure 1. Golgi pathology in motor neurons of *pmn* mice. (**A**) Golgi architecture assessed by immunofluorescence using MG160 in wild-type and *pmn* motor neurons. The middle row shows a 3D surface modeling illustrating Golgi fragmentation and the lower row demonstrates the strong reduction in Golgi area (atrophy) in *pmn* motor neurons. (**B**) Increased number of Golgi elements labeled with MG160 in *pmn* motor neurons after 3D modeling (mean $\pm$ SD, $n = 12$ motor neurons per genotype, ***$P < 0.0001$ by Student's *t*-test). (**C**) Reduced cross-sectional area of MG160-labeled Golgi elements in *pmn* motor neurons as assessed by immunofluorescence (mean $\pm$ SD, $n = 50$ motor neurons per genotype, **$P < 0.001$ by Student's *t*-test, unpaired, unequal variance). (**D**–**E**). Sizes of cell area and nuclear area measured, respectively, by VAChT immunofluorescence and DAPI staining are not statistically different between wt and *pmn*. (**F**) Electron microscopy showing an overview of a wild-type motor neuron (Day 35) with nucleus (N), nucleolus (No) and numerous Golgi profiles (arrows). Typical Golgi profiles in wild-type can be distinguished from partially vesicular, completely vesicular and remnant Golgi profiles in *pmn* motor neurons. (**G**) Quantification of Golgi profiles from the indicated categories in wild-type and *pmn* motor neurons at Day 15 and Day 35. Golgi profiles analyzed per time point: $n = 287$ (Day 15), $n = 372$ (Day 35). For each category and time point the difference between wt and *pmn* was statistically different, $P < 0.05$, Student's *t*-test, unpaired. Scale bar 10 μm (A), 200 nm (C).
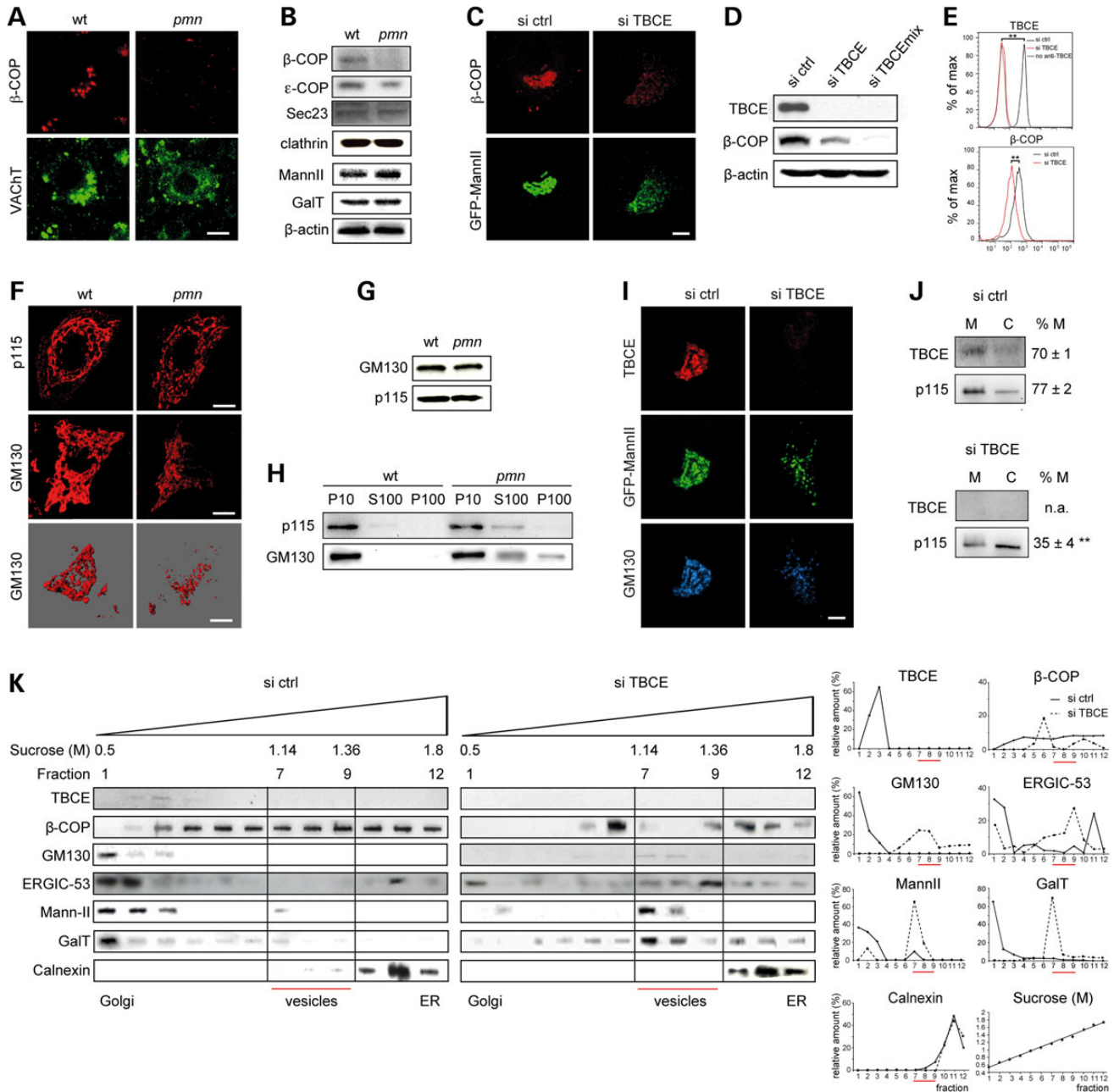
Figure 2. Defective COPI vesicle formation and tethering in mutant *pmn* and TBCE-depleted NSC34 motor neurons. (**A**) Confocal microscopy showing decreased β-COP immunoreactivity in a *pmn* motor neuron identified by vesicular acetylcholine transporter (VAchT) expression, as compared with a wild-type motor neuron at age 25 days. At least 100 motor neurons were analyzed from each lumbar spinal cord ($n = 3$ mice per genotype). (**B**) Western blot analysis of *pmn* lumbar spinal cords at age 25 days showing reduced levels of β-COP and ε-COP but normal levels of Sec23 and clathrin as compared with wild-type. Levels of MannII and GalT are also similar between *pmn* and wild-type. Western blots were performed using samples from three pairs of *pmn* and wt litter mice. Repeating the experiment twice gave similar results. (**C**) Confocal microscopy demonstrating decreased β-COP immunoreactivity in a TBCE-depleted NSC34 motor neuron with GFP-MannII-labeled Golgi fragmentation, as compared with a control neuron at 4 days in vitro (DIV) after transfection. (**D**) Western blot analysis of NSC34 motor neuron cultures showing decreased levels of β-COP after efficient TBCE depletion with si TBCE or si TBCE mix as compared with control. (**E**) Flow cytometry showing complete TBCE depletion in NSC34 motor neurons (upper panel), as compared with control cells incubated without primary antibody, and significant reduction of cellular β-COP levels (lower panel). $T(x) > 4$, $^{**}P < 0.01$ by χ^2 test. (**F**) Decreased p115 and GM130 immunoreactivity at Golgi membranes of *pmn* motor neurons as compared with wild-type siblings (upper rows). 3D-modeling of GM130 membranes (lower rows) confirms Golgi fragmentation in *pmn*. (**G**) Western blots demonstrating similar total levels of GM130 and p115 in *pmn* and wild-type spinal cords. (**H**) Subcellular fractionation showing pathological redistribution of GM130 and p115 from P10 fraction (membranes) to S100 (cytosol) and for GM130 also to P100 (membrane fragments, vesicles) in *pmn* spinal cord extracts, $n = 3$ independent experiments. (**I**) Confocal microscopy showing decreased GM130 immunoreactivity at fragmented Golgi (GFP-MannII) in TBCE-depleted NSC34 cell as compared with control cell. (**J**) Cell fractionation showing lower p115 recruitment to membranes in TBCE-depleted cells, as compared with controls. Protein expression in membrane (M) and cytosol (C) is quantified relative to total, %M = M/(M + C), mean $\pm$ SD, $^{**}P < 0.001$ by Student's *t*-test. na, not applicable, $n = 3$ independent experiments. (**K**) Sucrose density fractionation. In control cells, Golgi membranes are identified in fractions 1–4 by TBCE, MannII and GM130, vesicles in fractions 7–9 according to their sucrose density of 1.14–1.36 M (21) and ER membranes in fractions 10–12 by Calnexin. In TBCE-depleted cells, GM130 is completely lost from Golgi membranes, β-COP is specifically lost from vesicle fractions and ERGIC-53, MannII as well as GalT peak in vesicle fractions. Plots showing relative protein content per fraction (right panels) are representative of ≥ 2 independent experiments. Sucrose concentration in each fraction was measured by enzymatic assay. Scale bars 10 μm.

mediates Golgi vesiculation in *pmn* and TBCE-depleted motor neurons.

In the early secretory pathway, COPII vesicles normally fuse with themselves (25) and the ER/Golgi intermediate compartment (ERGIC) (26). β-COP-depletion is known to cause fragmentation of the ERGIC into vesicular structures containing ERGIC-53 (27) and Golgi-resident enzymes, such as GalT (22). In line with this, we found that ERGIC-53 and GalT are completely shifted to vesicle fractions in TBCE-depleted cells (Fig. 2K), suggesting that the accumulating vesicles represent ERGIC fragments and COPII vesicles unable to fuse.

Loss of TBCE leads to increased levels of Golgi v-SNAREs but impaired vesicle fusion

The fusion of COPI and COPII vesicles with their target membranes is mediated by the pairing of ER/Golgi v-SNAREs with cognate t-SNAREs (28). The vesicle accumulation in *pmn* and TBCE-depleted motor neurons might therefore suggest an impaired SNARE pairing. To test this, we assessed the formation of the two known ER/Golgi SNARE pairs GS28/Syntaxin 5a (29) and GS15/Ykt6 (30). By western blot, the total levels of the t-SNAREs Syntaxin 5a and Ykt6 (Fig. 3A) remain unchanged in *pmn* spinal cords whereas the levels of the v-SNAREs GS15 and GS28 are increased by >10-fold in *pmn* when compared with wild-type spinal cords (Fig. 3A). The level of the endosomal v-/t-SNAREs Vti1a/Syntaxin 6 remains unaffected demonstrating specificity (Fig. 3A). The increase in GS28 and GS15 levels in *pmn* versus wild-type motor neurons is also documented by immunofluorescence (Fig. 3B, upper rows). Quantitative polymerase chain reaction analyses showed no increase in GS15 and GS28 mRNA levels in *pmn* spinal cords at various time points (Supplementary Material, Fig. S2), suggesting that the increase in v-SNARE protein levels is due to enhanced protein stability or reduced protein degradation rather than to transcriptional up-regulation.

ER/Golgi v-SNAREs are recycled back to the ER by COPI vesicles (31,32) and loss of β-COP in *pmn* and TBCE-depleted cells might impede this recycling. To assess v-SNARE recycling, we examined the distribution of GS15 and GS 28 that accumulate in small dispersed puncta, as shown by 3D modeling (Fig. 3B, lower rows). These puncta likely correspond to Golgi vesicles or groups of Golgi vesicles as both v-SNAREs are shifted to vesicle fractions in TBCE-depleted fractionated cells (Fig. 3C), suggesting that loss of TBCE function impairs v-SNARE recycling to the ER.

To investigate why the v-SNARE-loaded Golgi vesicles accumulate instead of fusing, we assessed v-/t-SNARE pairing by immunoprecipitation and found that in TBCE-depleted cells GS15/Syntaxin 5a and GS28/Syntaxin 5a complexes are less abundant than in control cells (Fig. 3D upper rows), whereas unpaired GS15, GS28 and Syntaxin 5a are more abundant (Fig. 3D, lower rows). High resolution confocal imaging and pixel per pixel analysis supported that GS28/Syntaxin 5a signals are dissociated in TBCE-depleted cells but overlapping in control cells (Fig. 3E). Taken together, these data suggest that ER/Golgi SNARE pairing and recycling is strongly impaired in the absence of TBCE despite the increased protein levels of GS15 and GS28.

Golgi vesiculation in *pmn* motor neurons is caused by loss of TBCE and not a consequence of neuronal damage

Since Golgi fragmentation is one of the earliest pathological features of degenerating motor neurons in ALS (4), we thought to determine the onset and kinetics of Golgi vesiculation in *pmn* mice. Motor neuron disease in *pmn* mice first manifests at Day 15 with skeletal muscle paresis and atrophy and leads to the animal's death 3 weeks later (13). We here demonstrate that the loss of myelinated fibers in the phrenic motor nerve starts at Day 15 and then continues progressively (Supplementary Material, Fig. S3), in line with our earlier studies (20,33). We therefore monitored Golgi vesiculation in *pmn* and control litter mice at two presymptomatic stages (Days 5 and 10), disease onset (Day 15), midstage (Day 25) and endstage (Day 35). Altered GM130 and GS28 immunofluorescence in motor neurons is first detected at Day 10 (Fig. 4A–B), 5 days before first clinical and histopathological alterations. GM130 and GS28-labeled Golgi vesiculation then progressively affects the majority of motor neurons (Fig. 4A–B), matching a continuous rise of the v-SNARE levels in *pmn* spinal cords (Fig. 4C).

The presymptomatic onset of Golgi vesiculation in *pmn* mice suggests that this phenomenon is not a simple consequence of motor neuron damage. We tested this by unilateral transection of the sciatic nerve in wild-type mice and analysis of the retrogradely labeled lesioned motor neurons (Fig. 4D–F). Both p115 labeling (Fig. 4D–E) as well as β-COP, GS15 and GS28 protein levels (Fig. 4F) are unaffected in the lesioned motor neurons when compared with unlesioned ones, indicating that Golgi vesiculation in *pmn* motor neurons is not a consequence of motor neuron damage but may be a contributor to the disease.

To demonstrate that Golgi vesiculation in *pmn* motor neurons is due to loss of TBCE function, we complemented *pmn* mice with wild-type TBCE transgenes (18), which partially or completely restore TBCE expression at the Golgi apparatus (Fig. 4G–I). Transgenic TBCE complementation restores normal p115 labeling in individual motor neurons (Fig. 4G–H) and rescues the pathological spinal cord levels of β-COP, GS15 and GS28 (Fig. 4I). Transgenic TBCE complementation also normalizes the pathologically increased number of GS28-labeled Golgi elements in motor neurons of *pmn* mice, as shown by quantitation of 3D Golgi modelings (Fig. 4J–K). Whereas the number of small GS28-labeled Golgi elements increases in *pmn* motor neurons, it goes down to wild-type levels upon TBCE transgene expression in both lines of transgenic TBCE *pmn* mice, indicating full rescue of Golgi vesiculation. Taken together, these data indicate that loss of TBCE function in *pmn* motor neurons is responsible for Golgi vesiculation.

TBCE is instrumental for the nucleation and growth of Golgi-derived microtubules

How may loss of TBCE function cause Golgi vesiculation? According to previous studies (16), TBCE is essential for the folding of α-tubulin and its polymerization into microtubules. Tubulin polymerization in differentiated neurons mainly takes place at non-centrosomal sites (34) such as the Golgi (35,36) where TBCE is localized (18). We therefore searched for defects in Golgi-associated microtubules containing detyrosinated (Δ-Tyr) tubulin (37) and found that these are greatly diminished
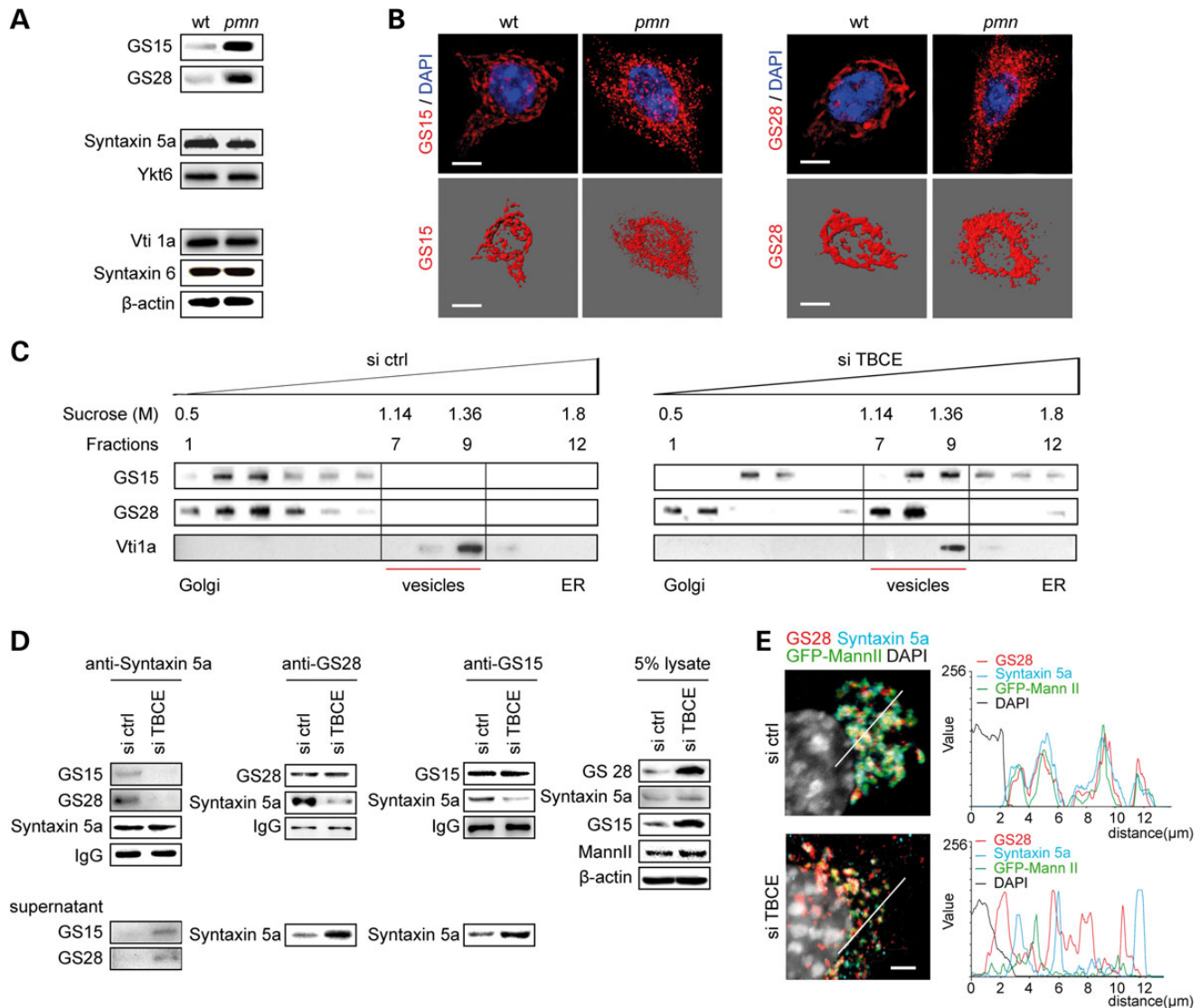
Figure 3. TBCE-linked Golgi vesiculation is associated with defective SNARE pairing and recycling. (**A**) Western blots showing a drastic increase in Golgi v-SNAREs GS15 and GS28 in *pmn* spinal cord but normal expression of the corresponding t-SNAREs Syntaxin 5a and Ykt6 as compared with wild-type siblings. Expression of endosomal SNARE pairs Vti1a/Syntaxin 6 and also of MannII and GalT is unaltered in *pmn*. (**B**) Confocal imaging (upper rows) and 3D modeling (lower rows) reveal accumulation of GS15 and GS28 in small vesicle-like puncta of *pmn* motor neurons. (**C**) Sucrose gradient fractionation showing a shift of GS15 and GS28 to vesicle fractions in TBCE-depleted cells. The control protein Vt1a is not shifted. Data are representative of ≥2 independent experiments. (**D**) Immunoprecipitation analysis of v-/t-SNARE complexes. Reduced levels of GS15/Syntaxin 5a and GS28/Syntaxin 5a complexes (upper panels) but increased amounts of unpaired SNAREs (lower panels) in TBCE-depleted cells as compared with control cells. Controls: MannII and β-actin in cell lysates, IgG in immuno-precipitates. Two independent experiments gave similar results. (**E**) High resolution confocal imaging and fluorescent line profiles showing dissociated GS28/Syntaxin 5a signals in TBCE-depleted cells as compared with overlapping signals in control cells, $n = 20$ cells analyzed per condition. Scale bars 10 μm (B), 5 μm (E).

in mutant *pmn* (Fig. 5A) and TBCE-depleted motor neurons (Fig. 5B–C). To confirm that TBCE is required for the nucleation and growth of Golgi-derived microtubules, we performed washout experiments after treatment with the microtubule-disrupting drug nocodazole (10 μM, 5 h). Nocodazole causes Golgi fragmentation into ministacks (5,6) but does not displace TBCE from the Golgi membrane (Fig. 5D). In control cells, small microtubule asters begin to form immediately after nocodazole washout at dispersed Golgi profiles (Fig. 5E). These microtubules then grow rapidly (Fig. 5F) and reach neighboring Golgi profiles (Fig. 5E, G), leading to re-formation of a compact Golgi ribbon within 200 min (Supplementary Material, Fig. S4). In TBCE-depleted

cells however, Golgi-derived microtubules are rare (Fig. 5E), grow much slower than in control cells (Fig. 5F) and only rarely reach neighboring Golgi profiles (Fig. 5E, G) leaving the Golgi disrupted at all time points (Supplementary Material, Fig. S4). These data indicate that TBCE is required for the nucleation and growth of Golgi-derived microtubules.

Accumulation of soluble α-tubulin is not sufficient to trigger Golgi vesiculation

During tubulin folding, α- and β-tubulins first interact with the chaperone proteins prefoldin (38) and cytosolic chaperonin

(39), thus generating tubulin folding intermediates (16). α-tubulin folding intermediates interact with tubulin chaperones TBCB and TBCE and β-tubulin folding intermediates with TBCA and TBCD (16,17). Finally, TBCE/α-tubulin, TBCD/β-tubulin and TBCC form a supercomplex that releases native α/β-tubulin heterodimers competent for polymerization into microtubules (40). In line with the function of TBCE in this pathway, we found that TBCE-depleted NSC34 cells contain more soluble α-tubulin (Fig. 6A), less polymerized α-tubulin (Fig. 6A), and alterations of cellular microtubules (Fig. 6C–D). These changes are closely associated with the molecular and structural stigmata of Golgi vesiculation (Fig. 6B–D).

To determine whether an increase in soluble α-tubulin can trigger Golgi vesiculation, we expressed the folding-defective α-tubulin mutant TUBA1 R264C which is unable to stably interact with TBCB (41). In contrast to its wild-type counterpart, flag-tagged mutant TUBA1 is not efficiently polymerized into cellular microtubules (Fig. 6E, H) and accumulates in a soluble form (Fig. 6E). Mutant TUBA1 significantly increases the cellular levels of soluble α-tubulin (Fig. 6F), similarly to TBCE depletion (Fig. 6A), but without affecting the polymerization of endogenous α-tubulin (Fig. 6F) or the structure of the residual microtubule network (Fig. 6H–I). Strikingly, expression of mutant TUBA1 does not alter β-COP, GS15 and GS28 levels (Fig. 6G) or Golgi structure (Fig. 6H–I), indicating that mutant TUBA1 expression is not sufficient to drive Golgi vesiculation. The differential effects of mutant TUBA1 expression and TBCE depletion strongly suggest that Golgi vesiculation is caused by loss of microtubules rather than by accumulation of soluble α-tubulin.

Golgi maintenance depends on an ARF1/TBCE-mediated cross-talk that coordinates COPI vesicle formation and tubulin polymerization at the Golgi

Our data raise the hypothesis that TBCE maintains Golgi structure by adjusting the polymerization of Golgi-derived microtubules to the formation of COPI vesicles. To begin to test this, we modulated the activity of ARF1, the small GTPase that controls COPI vesicle formation (1). Inhibiting ARF1 activity with brefeldin A not only reduces the levels of β-COP at the Golgi, but also shifts TBCE into the cytosol and decreases the number of Golgi-derived microtubules (Supplementary Material, Fig. S5A–B), suggesting that ARF1 regulates TBCE activity.

We next enhanced ARF1 function by (over)expressing wild-type ARF1 or the constitutively active ARF1 mutant Q71L. Both forms of ARF1 accumulate at the Golgi and recruit β-COP (Fig. 7A), as expected. Remarkably, they also lead to an increased recruitment of TBCE to the Golgi membrane, as observed by immunolabeling (Fig. 7A, arrows on right panels), cell fractionation (Fig. 7B) and flow cytometry (Fig. 7C) and to increased polymerization of Golgi-derived microtubules (Fig. 7A and C). Overall, ARF1 Q71L is significantly more effective than ARF1 wt (Fig. 7C). Taken together, these data suggest a cross-talk between ARF1 and TBCE that coordinates tubulin polymerization and COPI formation at the Golgi.

To test whether this cross-talk is involved in Golgi maintenance, we attempted to rescue TBCE-linked Golgi alterations with ARF1. Remarkably, overexpression of ARF1 Q71L after

TBCE knockdown strongly prevents alterations of Golgi-derived microtubules (Fig. 7D–E) and rescues defective Golgi architecture labeled by β-COP and GM130 (Fig. 7D–E and data not shown). Flow cytometry suggests that this occurs through ARF1-mediated stabilization of membrane-bound TBCE (Fig. 7F). These data show that defective ARF1/TBCE cross-talk causes Golgi fragmentation in motor neurons.

DISCUSSION

We here report a novel ARF1/TBCE-mediated cross-talk (Fig. 7G) in which membrane-bound active ARF1 catalyzes COPI coat assembly and recruits TBCE to the Golgi membrane where TBCE drives the nucleation and polymerization of Golgi-derived microtubules. We hypothesize that these microtubules then stabilize the COPI coat through their reported interaction with the β-COP subunit (7). The ARF1/TBCE cross-talk is reminiscent of the regulation of the tubulin-binding co-factor TBCD by the ARF1-related GTPase ARL2 (42). It also mirrors interactions between COPII and the microtubule-dependent motor protein dynein at ER exit sites (43), and between clathrin and actin at the trans Golgi network (44,45), illustrating emerging signaling pathways between vesicular coats, cytoskeleton and motor proteins that ensure efficient coordination of carrier formation and transport in the secretory pathway.

How does an interrupted cross-talk between ARF1 and TBCE cause Golgi fragmentation? We show that absence of TBCE causes loss of Golgi-derived microtubules, β-COP degradation and diminished membrane-recruitment of tethering factors p115/GM130. The degradation of β-COP, ε-COP and possibly other COPI subunits impedes the function of the ER/Golgi intermediate compartment as the target for COPII-derived vesicles (25,26), resulting in accumulation of the latter. This scenario of Golgi fragmentation (Fig. 7G) is recapitulated by β-COP depletion, causing accumulation of small vesicles containing Golgi enzymes at the cell center (22) and redistribution of GM130 (24).

How does loss of TBCE function cause the increased level of Golgi v-SNAREs GS15 and GS28? There are two possibilities. First, GS28 is known to be recycled by COPI vesicles (46) and to be degraded by the proteasome after interaction with the ubiquitin-like (UBL) protein GATE-16 and its regulator ORP7 (47,48). The *pmn* mutation results in the incorporation of the v-SNAREs in COPII vesicles, possibly away from GATE-16 and its function in proteasomal degradation, hence leading to their accumulation. Second, TBCE itself contains a C-terminal UBL domain which is structurally similar to GATE-16 (T. Levine, personal communication) and might thus directly participate in the v-SNARE degradation. The Trp524>Gly mutation in *pmn* would destabilize the UBL domain inhibiting its interaction with the proteasome (49) leading to the v-SNARE increase.

Does altered COPI vesicle formation or trafficking cause Golgi fragmentation in other neurodegenerative diseases than *pmn*? It may be the case in mice mutated in the COPI subunit δ-COP/Archain with Purkinje cell degeneration (50) and in mice mutated in the β-COP-interacting protein Scyl1 such as *muscle deficient* (51,52) or Scyl1 KO (53) with motor neuron degeneration which, however, need to be investigated for potential Golgi alterations. It is likely the case in motor neurons of mutant
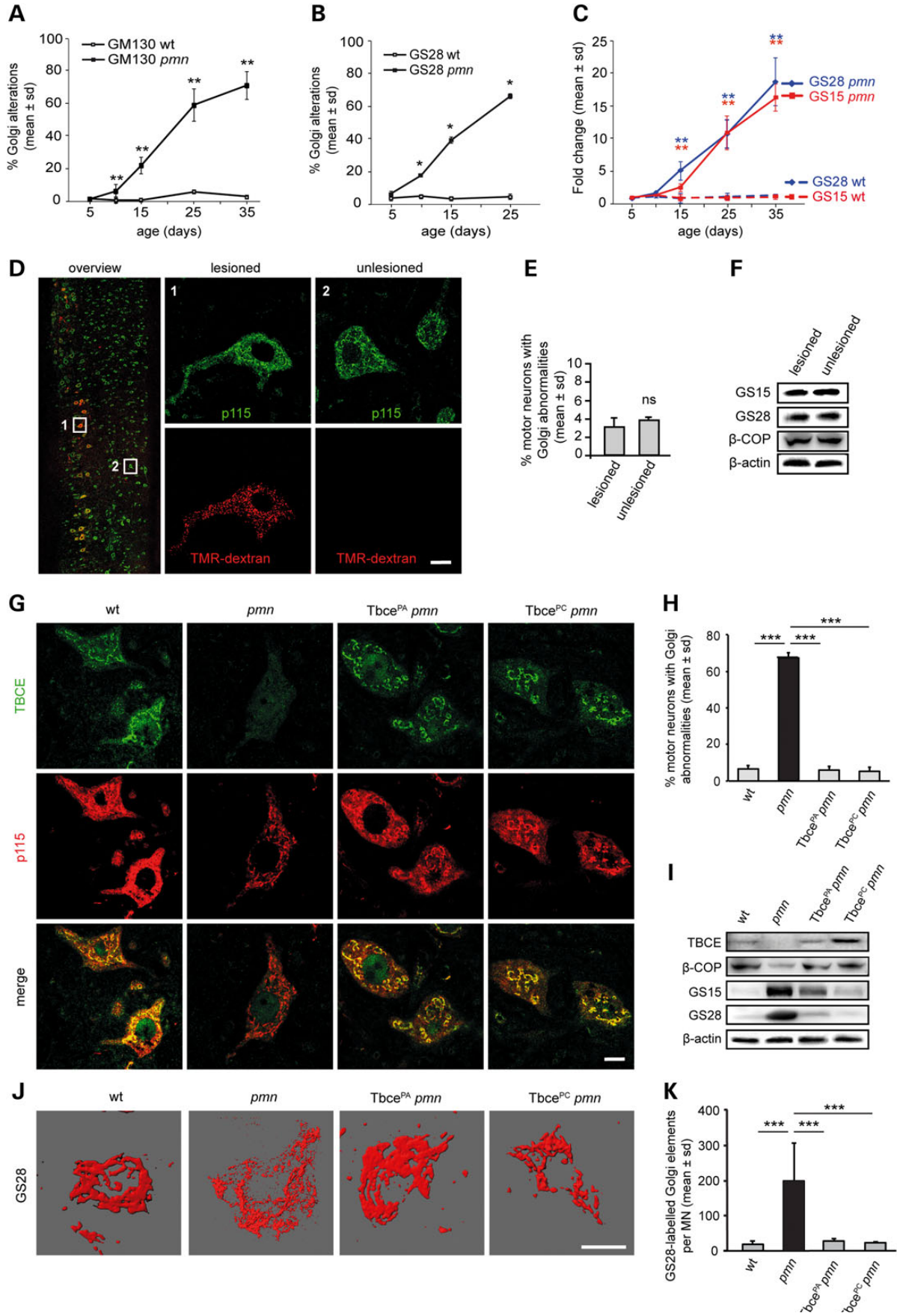
SOD1 mice since these display Golgi fragmentation and up-regulation of the microtubule-depolymerizing protein stathmin (8) together with similar dysregulation of β-COP, GS15 and GS28 (Supplementary Material, Fig. S6A-D) and similar GS15- and GS28-labeled Golgi vesiculation (Supplementary Material, Fig. S6E–F) as *pmn* mice. Defective coordination of vesicle formation and trafficking may thus cause Golgi fragmentation in human SOD-linked ALS and other neurodegenerative disorders.

What may be the contribution of altered COPI vesicle trafficking to motor neuron degeneration and dysfunction? Blocking COPI formation in neuronal cultures by inhibiting ARF1 causes collapse of growing axons (54), suggesting a critical role of COPI vesicles in axon growth or maintenance. The COPI subunit α-COP has been shown to interact with survival motor neuron (SMN), the protein deficient in spinal muscular atrophy, and to co-traffic with SMN in motor axons (55). Interrupting α-COP–SMN interactions leads to SMN accumulation at the Golgi (56), reduced neurite outgrowth (57) and growth cone defects similar to those observed after pharmacological Golgi fragmentation (56). Furthermore, the COPI subunits α-, β- and γ-COP bind numerous mRNAs (58,59) at least some of which require microtubules for their axonal transport (58). The Golgi apparatus is also responsible for packaging precursors of synaptic vesicles which are lost at an early disease stage in mutant SOD1 (60), SMN (61) and *pmn* mice (B.S., G.H., unpublished data). Defective coordination between the polymerization of microtubules and the formation of COPI vesicles may thus compromise the transport of critical axon and synapse constituents and thereby contribute to motor neuron degeneration and dysfunction.

MATERIALS AND METHODS

Antibodies and reagents

Primary antibodies were as follows [supplier, dilution in immunofluorescence (IF), western blot (WB) and cytometry (Cyt)]: TBCE [rabbit SA53 (18)], IF 1:300, WB 1:500, Cyt 1:50), TBCE (Abnova, IF 1:200), FLAG (Sigma, IF 1:1000, WB 1:2000), GFP (Roche, WB 1:2000), HA (Roche, WB 1:1000, cytometry 1:750), VAChT (Sigma, IF 1:2000), ChAT (Chemicon, IF 1:100), GM130 (Becton Dickinson, IF 1:300, WB 1:500), p115, GS15, GS28, Rab5, Syntaxin 6, Calnexin, Clathrin, Vti1a, (Becton Dickinson; IF 1:300, WB 1:1000), Syntaxin 5a (Abcam, WB1:1000), Sec23 (Abcam 50672, WB 1:1000), β-COP (Abcam, WB 1:2000, IF 1:500, Cyt 1:1000), β-COP (Dr R. Duden, University of Lübeck, WB 1:1000), MG160 (Abcam, IF: 1:500), ARF1 (Dr R.A. Kahn, Emory University, WB 1:1000), Ykt6 (Dr J.C. Hay, University of Michigan, WB 1:2000), MannII (Covance, WB 1:1000), GalT (PTG, WB 1:1000), KDEL (StressGen, IF 1:500), α-tubulin (Sigma, IF 1:2000, WB 1:5000), acetylated-tubulin (Sigma, WB 1:2000), β-actin (Sigma, WB 1:5000), α-tubulin-fluorescein isothiocyanate (FITC) (Sigma, Cyt 1:2000), β$_{III}$-tubulin (TuJ1, Babco, IF 1:2000, WB 1:10000), Δ-Tyr-tubulin (Dr A. Andrieux, IF 1:5000, WB 1:10000, Cyt 1:1000), Tyr-tubulin (Dr A. Andrieux, WB 1:2000). Fluorochrome-conjugated secondary antibodies were from Molecular Probes (Carlsbad, CA) and horse radish peroxidase-conjugated secondary antibodies from Jackson Immuno Research (West Grove, PA).

Small interfering (si) RNA duplexes against mouse TBCE (NM_178337, refs D-057655-00 and M-057655-01) or luciferase control (ref P-002099-01-20) were purchased from Dharmacon (Chicago, IL).

si TBCE 5′-GUAGAAGAGUUGAAGUUAA
si TBCE mix 5′-GUAGAAGAGUUGAAGUUAA,
5′-CCACGAAGGUACUAUGUAU,
5′-UACCUCAAGUCUAACAAUA,
5′-CUAGAAACCCUUUGAGCAA
si luciferase 5′-CAUUCUAUCCUCUAGAGGAUG

Plasmid expression vectors contained the following cDNAs: GFP-MannII (Dr M. Bornens, Institut Curie, Paris), TUBA1A wt or TUBA1A R264C (Dr J. Chelly, Institut Cochin, Paris), ARF1 wt, Q71L and T31N (Dr J. Donaldson, NIH, Bethesda).

Additional reagents were from the following suppliers: phosphate buffered saline (PBS), Hank's balanced salt solution, trypsin, culture media and supplements (Invitrogen, Carlsbad,

Figure 4. Kinetics, specificity and TBCE-mediated rescue of Golgi vesiculation in *pmn* motor neurons. (**A**–**B**) Kinetics of Golgi alterations labeled by immunofluorescence for GM130 (A) or GS28 (B) in *pmn* and wild-type motor neurons, *n* > 200 motor neurons from at least two mice per genotype and time-point, **P < 0.01 by Student's *t*-test. (**C**) Kinetics of GS15 and GS28 levels in *pmn* and wild-type spinal cord extracts analyzed by western blot. Fold changes are expressed relative to levels at Day 5. Each time point represents *n* = 3 spinal cords per genotype analyzed each by two independent densitometric scans. * P < 0.05 by Student's *t*-test., **P < 0.01 by Student's *t*-test. (**D**) Confocal imaging showing the absence of Golgi alterations after axotomy. Sciatic nerves of 35-day-old normal mice were unilaterally transected, motor neurons retrogradely labeled with Tetramethylrhodamin (TMR)–dextran and lumbar spinal cord sections immunolabeled for p115. The overview in the frontal plane shows motor neurons on the lesioned and unlesioned side. The zooms demonstrate absence of Golgi pathology in lesioned motor neurons, as compared with unlesioned motor neurons. (**E**) No significant Golgi alterations in lesioned motor neurons. *P* = 0.34 (ns, non-significant by Student's *t*-test), *n* = 251 (lesioned), *n* = 275 (unlesioned) motor neurons from a total of three animals. (**F**) Western blots showing similar levels of β-COP, GS15 and GS28 in lumbar spinal cord hemisegments from the lesioned and unlesioned side. (**G**) Confocal imaging showing rescue of Golgi alterations in *pmn* mice by transgenic complementation with wild-type TBCE. Lumbar spinal cord cross sections from 35-day-old wild-type, *pmn*, transgenic Tbce^{PA} *pmn* and Tbce^{PC} *pmn* mice were immunolabeled for TBCE and p115. Loss of TBCE expression in *pmn* motor neurons is associated with reduced p115 immunolabeling at Golgi membranes. Transgenic TBCE expression in motor neurons of Tbce^{PA} *pmn* and Tbce^{PC} *pmn* mice restores normal p115 immunolabeling. (**H**) Rescue of p115-labeled Golgi alterations in motor neurons of transgenic Tbce^{PA} *pmn* and Tbce^{PC} *pmn* mice. Number of motor neurons and mice analyzed per genotype: wt *n* = 390 (four mice), *pmn* 397 (four mice), Tbce^{PA} *pmn* *n* = 275 (3 mice), Tbce^{PC} *pmn* *n* = 321 (three mice). Statistical significance ***P < 0.001 by one-way ANOVA and Tukey's *post hoc* test: significant for *pmn* versus wt, Tbce^{PA} *pmn* versus *pmn*, and Tbce^{PC} *pmn* versus *pmn*, Tbce^{PA} *pmn* versus wt, not significant for Tbce^{PC} *pmn* versus wt, Tbce^{PA} *pmn* versus *pmn* and Tbce^{PC} *pmn* versus Tbce^{PA} *pmn*. (**I**) Transgenic rescue of pathological β-COP, GS15 and GS28 expression analyzed by western blot in lumbar spinal cord of Tbce^{PA} *pmn* and Tbce^{PC} *pmn* mice as compared with wild-type and *pmn* mice. Data are representative of three independent tissue samples per genotype. Two independent experiments gave similar results. (**J**) Rescue of Golgi vesiculation by transgenic TBCE complementation. 3D modelings show GS28-labeled Golgi elements in lumbar motor neurons of the indicated genotypes. (**K**) Rescue of the number (mean ± SD) of GS28-labeled Golgi elements determined by 3D-modeling. Number of motor neurons counted by an observer blinded to the genotypes: wt *n* = 12, *pmn* *n* = 12, Tbce^{PA} *pmn* *n* = 13, Tbce^{PC} *pmn* *n* = 12, each from two mice per genotype. Statistical significance *P* < 0.0001 between groups by Kruskal–Wallis test and Dunn's *post hoc* test for *pmn* versus wt, Tbce^{PA} *pmn* versus *pmn* and Tbce^{PC} *pmn* versus *pmn*; not significant for Tbce^{PA} *pmn* versus wt, Tbce^{PC} *pmn* versus wt, and Tbce^{PA} *pmn* versus Tbce^{PC} *pmn*. Scale bars 10 μm.
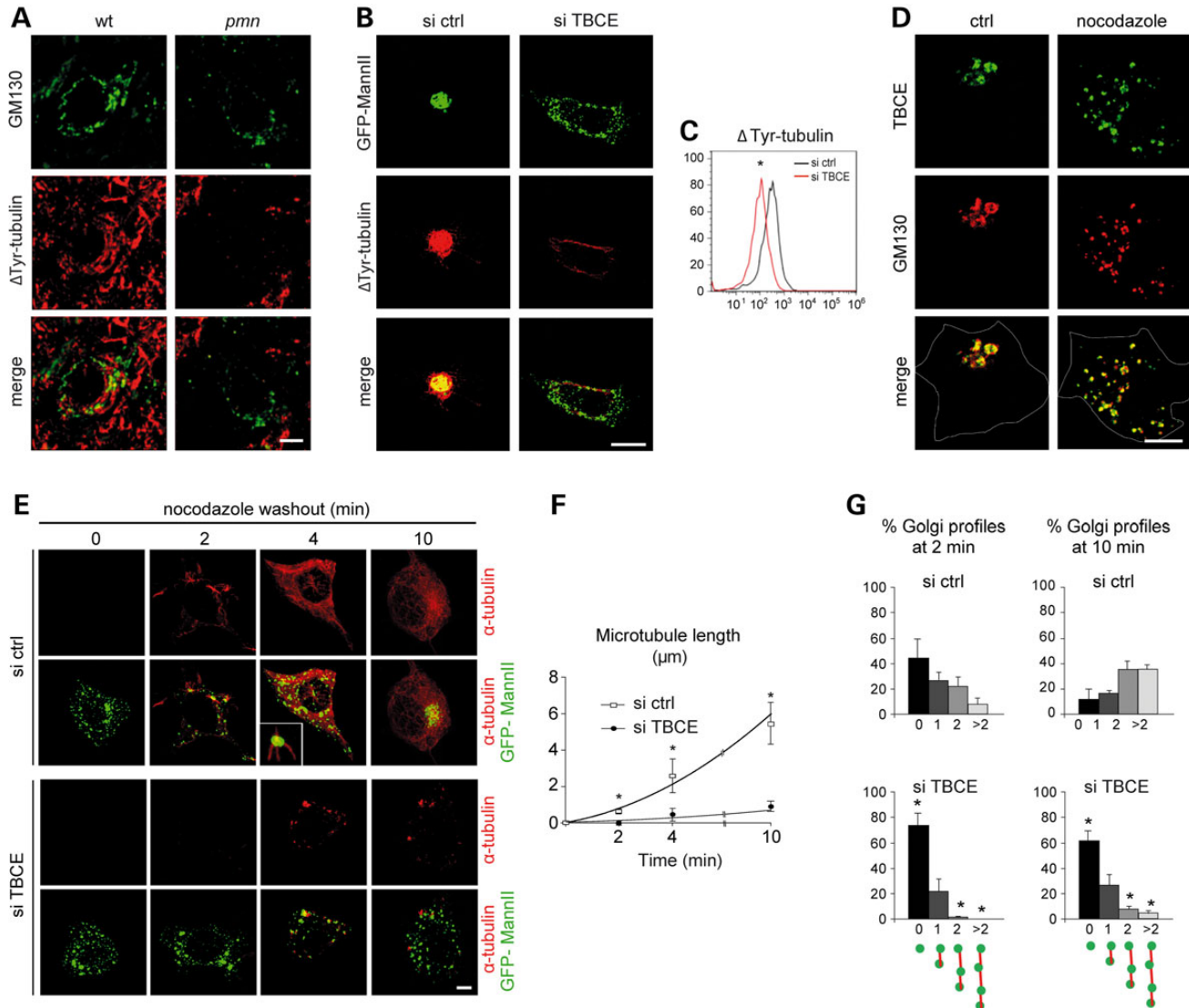
Figure 5. Defective polymerization of Golgi-derived microtubules in *pmn* and TBCE-depleted motor neurons. (**A**) Immunofluorescence showing that fragmentation of the GM130-labeled Golgi apparatus in motor neurons of 25-day-old *pmn* mice is associated with loss of Golgi-associated microtubules labeled for ΔTyr-tubulin, as compared with wild-type. (**B**) Loss of ΔTyr-tubulin-labeled microtubules in TBCE-depleted NSC34 motor neurons co-labeled with GFP-MannII, as compared with control. (**C**) Flow cytometry showing reduced levels of ΔTyr-tubulin-labeled microtubules after TBCE-depletion. (**D**) Immunofluorescence showing that TBCE remains associated with GM130-labeled Golgi profiles in nocodazole-treated NSC34 cells. (**E**) Immunofluorescence showing regrowth of microtubules from GFP-MannII-labeled Golgi profiles in control and TBCE-depleted NSC34 motor neurons after nocodazole treatment and washout. (**F**) Reduced growth rate of Golgi-derived microtubules in TBCE-depleted cells. Each point (means of mean $\pm$ SD) represents $n = 10$ cells per condition/time point and 10 randomly chosen microtubules per cell, $^{*}P < 0.05$ by Student's *t*-test. (**G**) Increased percentage of Golgi elements unlinked to microtubules in TBCE-depleted cells as compared with control cells after nocodazole washout. Golgi elements are classified into four categories. Mean $\pm$ SD, $n \approx 500$ profiles analyzed per time point and condition, $^{*}P < 0.05$ by Student's *t*-test.

CA), polyornithin, taxol, nocodazole (Sigma), Vectashield (Vector laboratories, Burlingame, CA), Complete protease inhibitors (Roche, Basel, Switzerland), Ketamine (Bayer, Leverkusen, Germany) and Xylazine (Mérial, Lyon, France), coverslips and Superfrost Plus glass slides (Menzel, Schwerte, Germany).

Mouse lines

Mutant *pmn* mice, TBCE[PA/+] *pmn* and TBCE[PC/+] *pmn* mice were maintained on a mixed background (C57/BL6; 129/SvJ) using intercrosses (>F8) and genotyped by PCR (18).

Axotomy and retrograde labeling of motor neurons

Mice were anesthetized by intraperitoneal injection of Ketamine (50 mg/kg) and Xylazine (10 mg/kg). Under a stereomicroscope, a skin incision was made, the sciatic nerve identified and cut at the hip level. A piece of hemostatic sponge (Spongostan, Ferrosan, Denmark) 2 × 2 × 2 mm in size was soaked in tetramethylrhodamine–dextran (Molecular Probes, 10% w/v in PBS) and applied to the proximal stump. The wound was closed with metal clips and an antibiotic prophylaxis with ampicillin administered. All experiments with animals were performed in strict compliance with French and European legislation.
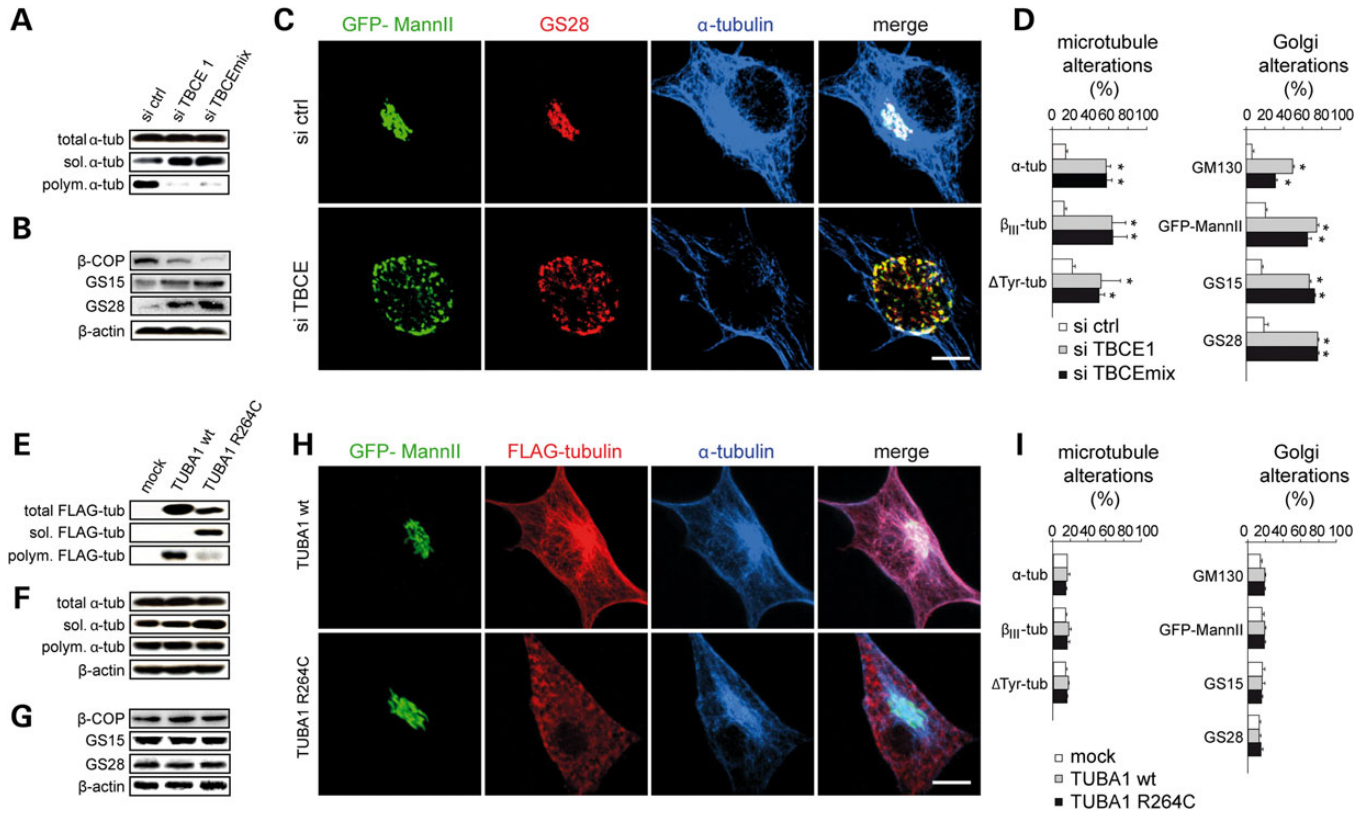
Figure 6. Tubulin polymerization, Golgi structure and vesicle markers after TBCE depletion or mutant α-tubulin expression. (**A**) Western blot showing that TBCE-depletion does not affect the total levels of α-tubulin but leads to a drastic decrease in the levels of polymerized α-tubulin and a significant increase in the levels of soluble α-tubulin (siTBCE 1: 1.6 ± 0.3-fold, siTBCE mix: 1.9 ± 0.1-fold, mean $\pm$ SD, Mann–Whitney test, paired). Soluble α-tubulin levels were quantified by densitometric analysis of six blots from three independent transfections. β-actin loading control is shown in panel B. (**B**) Decreased levels of β-COP in TBCE-depleted cells in comparison to control cells. Levels of GS15 and GS28 are increased in comparison to control by 7.4 ± 0.6 and 6.2 ± 0.3-fold (mean $\pm$ SD) respectively, as quantified by densitometric analysis of four independent experiments. (**C**) Confocal imaging showing that the α-tubulin-labeled microtubule alterations in TBCE-depleted cells are associated with Golgi alterations labeled with GFP-MannII and GS28, as compared with control. (**D**) Increased percentage of microtubule alterations labeled with α-, β_{III}- or ΔTyr-tubulin and Golgi alterations labeled with GM130, GFP-MannII, GS15, and GS28 in TBCE-depleted cells, as compared with control cells, mean $\pm$ SD, $n \geq 100$ cells per condition. Asterisks indicate statistical significance, $P < 0.05$ as measured by Student's t-test, unpaired, unequal variance. (**E**) Western blot analysis with anti-FLAG antibodies showing that expression of FLAG-tagged mutant α-tubulin (TUBA1 R264C) leads to increased levels of soluble mutant α-tubulin and decreased levels of polymerized mutant α-tubulin, in comparison to expression of FLAG-tagged wild-type α-tubulin (TUB1A wt). (**F**) Western blot with anti-α-tubulin antibodies showing a 1.6 ± 0.2-fold increase (mean $\pm$ SD) in the levels of soluble α-tubulin after TUBA1 R264C expression, as quantified by densitometric analysis of six independent blots; $P < 0.026$, Mann–Whitney test, paired, unequal variance. (**G**) Unaltered expression of β-COP, GS15 and GS28 in mutant TUBA1 R264C expressing cells. (**H**) Confocal imaging demonstrating that FLAG-tagged α-tubulin mutant TUBA1 R264C does not affect Golgi or microtubule structure. (**I**) Absence of microtubule or Golgi alterations in cells expressing mutant TUBA1 R264C α-tubulin, mean $\pm$ SD, $n \geq 100$ cells per condition. Scale bars 5 μm.

Confocal imaging, morphometry and 3D modeling

Images were obtained with an LSM 510 confocal microscope (Zeiss, Oberkochen, Germany). Motor neurons on spinal cord tissue cryosections were identified by staining for the motor neuron markers VAChT (vesicular acetylcholine transferase) or ChAT (choline acetyltransferase). Cells were imaged by confocal microscopy using a ×40 water immersion objective, an xy-resolution of 1024×1024 pixel, a z-interval of 0.3 μm and a mean scan depth of 30 μm.

Morphometric analyses were done with Metamorph software (Molecular Dynamics) using single confocal cross sections taken at the nuclear midplane. The boundaries of the ChAT-labeled cell soma and the DAPI-stained nucleus were manually delineated with the Metamorph drawing tool. Golgi surface area was automatically determined with the Metamorph morphometry tool by applying a fixed threshold to the MG160 signal.

Three-dimensional (3D) modelings of the Golgi apparatus were done with Imaris software (Bitplane, Zurich, Switzerland). Images were processed and Golgi membranes visualized using the IsoSurface mode of the Surpass module. The number of individual Golgi elements per motor neuron was determined in a blinded manner. Fluorescent line intensity profiles were determined with the linescan module of Zen software (Zeiss) on confocal z-stacks of NSC34 cells (z-interval 0.3 μm, scan depth 10 μm).

Electron microscopy

Deeply anesthetized mice were transcardially perfused with Sorensen's phosphate buffer (pH 7.4) followed by glutaraldehyde (2% v/v in cacodylate). Spinal cords were dissected out, post-fixed for 24 h and cut into small segments comprising the
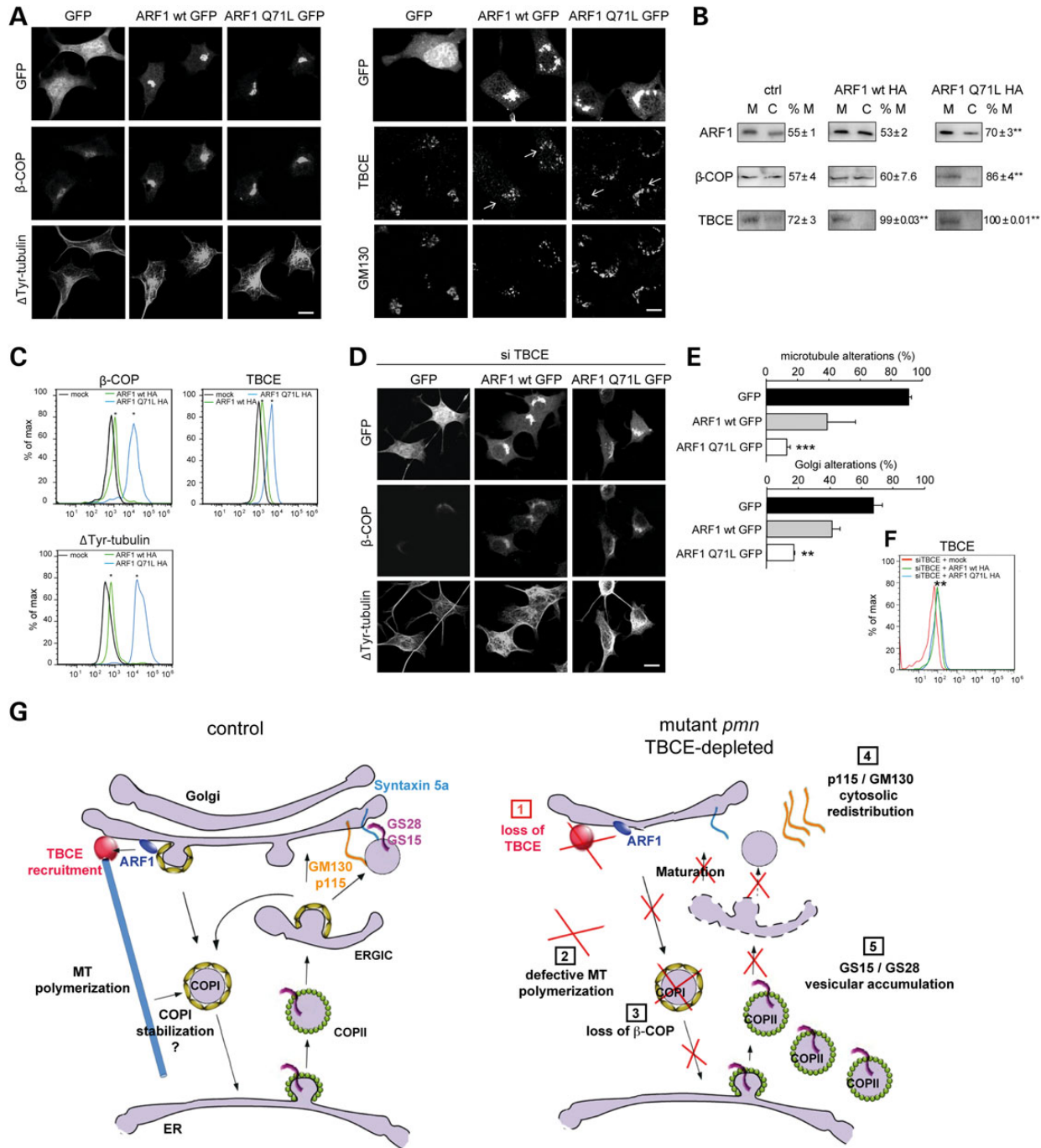
Figure 7. Role of an ARF1/TBCE-mediated cross-talk in Golgi maintenance. (**A**) Confocal imaging showing that expression of GFP-tagged ARF1 wt or ARF1 Q71L in NSC34 cells triggers a stronger β-COP signal and polymerization of more ΔTyr-tubulin-containing microtubules around the Golgi apparatus than GFP expression (left panels). GFP-tagged ARF1 wt and GFP-tagged ARF1 Q71L recruit TBCE to Golgi membranes labeled with GM130 (arrow, right panels). (**B**) Cellular fractionation. Expression of HA-tagged ARF1 wt or ARF1 Q71L stimulates recruitment of β-COP and TBCE from cytosolic (C) to membrane fractions (M). Relative protein expression is indicated as %M: M/(M + C), mean ± SD, $n = 3$ experiments, $**P < 0.001$, by Student's t-test. (**C**) Flow cytometry showing increased levels of β-COP, TBCE and ΔTyr-tubulin-containing microtubules after expression of ARF1 Q71L HA, in comparison to ARF1 wt HA or mock. Statistical significance $*$ARF1 wt HA versus mock $T(x) > 4$, $P < 0.01$; ARF1 Q71L HA versus ARF1 wt $T(x) > 28$, $P < 0.01$, by χ^2 test. (**D**) Confocal imaging reveals rescue of the pathologically decreased β-COP expression in siTBCE transfected cells by expression of GFP-tagged ARF1 wt or ARF1 Q71L, as compared with expression of GFP (upper and middle rows). Note also enhanced polymerization of ΔTyr-tubulin by expression of GFP-tagged ARF1 wt or GFP-tagged ARF1 Q71L (lower rows). (**E**) Rescue of microtubule or GM130-labeled Golgi alterations by ARF1 Q71L GFP in siTBCE-transfected cells (mean ± SD). Each experiment was done in triplicate conditions with $n > 50$ cells per condition. Statistical significance: $***P < 0.0002$ (microtubule alterations) and $**P < 0.0036$ (Golgi alterations) by Kruskal–Wallis test and Dunn *post hoc* test for ARF1 Q71L GFP/siTBCE versus GFP/siTBCE. (**F**) Flow cytometry showing increased levels of TBCE by (over)expression of ARF1 wt HA or ARF1 Q71L HA. Statistical significance $**$ARF1 wt HA-siTBCE wt versus mock siTBCE $T(x) > 26$, $P < 0.01$; ARF1 Q71L HA/si TBCE versus mock/si TBCE $T(x) > 26$, $P < 0.01$, by χ^2 test. (**G**) Model showing the ARF1/TBCE cross-talk which coordinates polymerization of Golgi-derived microtubules and COPI vesicle formation and the consequences of its disruption in mutant *pmn* and TBCE-depleted motor neurons. Scale bars 10 μm.

ventral spinal cord before processing for resin embedding (epon) following standard protocols. Sixty nanometer ultrathin cross sections were contrasted with uranyl acetate and visualized under a JEOL electron microscope. At least two lumbar spinal cords from each genotype were analyzed and three sections (each containing up to 30 motor neurons) were analyzed per time point. Motor neurons were recognized on the basis of their frequency (1:20), large size and pale nucleus. Within individual motor neurons, all Golgi profiles were categorized.

Cell culture

NSC34 motor neurons were cultured in DMEM supplemented with 10% (v/v) fetal calf serum at 37°C and 7.5% CO_2 and transfected with siRNAs and/or DNA plasmids using Lipofectamine 2000 (Invitrogen) as described (18).

Immunoblots and subcellular fractionation

Lumbar spinal cords from deeply anesthetized mice and NSC34 cells were homogenized in lysis buffer containing 50 mM Tris–HCl pH 7.5, 150 mM NaCl, 2 mM ethylenediaminetetraacetic acid (EDTA), 1% Triton X-100, Complete antiproteases and, for GM130, also 0.25% sodium dodecyl sulfate (SDS). 30 or 50 μg protein were subjected to SDS-polyacrylamide gel electrophoresis and blotted on Immobilon membranes (Millipore) which were processed by standard methods, reacted with ECL or ECL plus kits (Amersham) and revealed with XAR films (Kodak) or a Biorad imager. Band intensities were quantified by TotalLabQuant software.

Crude fractionation of membranes from lumbar spinal cord was done after tissue freezing (−80°C), thawing and homogenization in 50 mM 4-(2-hydroxyethyl)-1-piperazineethanesulfonic acid (HEPES), pH 7.4, 250 mM sucrose, 1 mM Mg acetate and protease inhibitors (Complete, EDTA-free). Lysates were homogenized using a Dounce homogenizer (15 passes) and centrifuged at 1 000 g for 10 min. The postnuclear supernatant was centrifuged at 10 000 g for 30 min at 4°C yielding a P10 pellet and the supernatant was centrifuged at 100 000 g (Beckman TLA-110) for 1 h at 4°C yielding an S100 supernatant and a P100 pellet.

For membrane fractionation on sucrose density gradients, cells were homogenized in an isotonic sucrose solution by 10 passages through a Dounce homogenizer and centrifuged at 1 000 g for 10 min. The postnuclear supernatants were centrifuged at 190 000 g (43 000 rpm) for 1 h in a Beckman SW60 Ti rotor; 12 fractions of 330 μl each were collected from top to bottom and equal volumes analyzed by immunoblot. Sucrose concentrations in fractions and standards were determined by an enzymatic assay (Sigma, ref. SCA-20) using a Biochrom WPA spectrophotometer. Subcellular fractionation of NSC34 cells into membrane and cytosolic fractions was done as described (21).

Microtubule re-growth assay

Growth dynamics of Golgi-derived microtubule were studied by modifying an earlier reported procedure (18). NSC34 cells transfected with siRNAs and a GFP-MannII plasmid were treated at 5 days in vitro (DIV) with nocodazole (10 μM, 5 h, 37°C). Nocodazole was then washed out with warm culture medium, and neurons further incubated at 37°C. At time intervals ranging from 0 to 200 min, cultures were rinsed with PHEM 60 mM piperazine-N,N'-bis(2-ethanesulfonic acid), 25 mM HEPES, 10 mM ethylene glycol tetraacetic acid, 2 mM $MgCl_2$, 1% formaldehyde (pH 6.9) and then treated for 3 min with PHEM containing 0.2% Triton X-100 and 20 μM taxol to extract soluble proteins and stabilize microtubules. Cells were fixed, blocked and counterstained for α-tubulin. After confocal imaging of entire cells, number and length of Golgi-derived microtubules were determined using Metamorph and ImageJ software respectively.

Immunoprecipitation

Transfected NSC34 cells from 6-well plates were harvested in PBS using a cell scraper and lysed on ice for 10 min in 50 mM Tris pH 7.5, 150 mM NaCl, 5 mM EDTA, 1% Triton X-100 and Complete protease inhibitors. After removal of cell debris, 300 μl of cell lysates were incubated with 3 μg antibodies and 30 μl protein G-magnetic beads (Millipore) on a tube rotator for 4 h. Supernatants and immune complexes were then collected using a magnetic stand holder.

Flow cytometry

Transfected cells were harvested at 3 DIV (ARF1) or 5 DIV (siTBCE), rinsed with PBS, centrifuged at 250g, washed with PHEM and treated for 3 min with PHEM containing 0.1% Triton X-100 and 20 μM taxol to extract soluble proteins and to stabilize microtubules. Cells were fixed for 15 min at RT by adding an equal volume of 8% (v/v) FA in PBS, rinsed in PBS, centrifuged and blocked for 30 min in 5% goat serum, 1% (w/v) BSA and 0.1% (v/v) Triton X-100. Cells were incubated for 1 h with primary antibodies and for 1 h with secondary antibodies or biotin/streptavidin reagents coupled to Alexa-594 (HA) or Alexa-488 (β-COP, TBCE and ΔTyr-tubulin). One thousand five hundred cells per duplicate sample and condition were analyzed with a FACS ARIA SORP (Becton Dickinson) and signals plotted with FlowJo software.

Statistical analyses

Each experiment was performed with several biological replicates, i.e. usually three pairs of wild-type and *pmn* mice and duplicate or triplicate cultures of control and siTBCE-transfected cells. All experiments were repeated once or twice. Data were analyzed with Microsoft Excel, SigmaStat 3.1 (Systat, Evanston, IL) or GraphPad Prism (GraphPad). Data from two groups showing Gaussian distribution were analyzed with Student's *t*-test; otherwise the Mann–Whitney *U* test was used. Data from more than two groups showing Gaussian distribution and equal variance were analyzed with one-way ANOVA test and Tukey's *post hoc* test; otherwise the Kruskal–Wallis test and Dunn *post hoc* test were used. Cytometry data were tested for significance with the $\chi 2$ test using FlowJo software.

SUPPLEMENTARY MATERIAL

Supplementary Material is available at *HMG* online.

ACKNOWLEDGEMENTS

FUNDING

REFERENCES

1. Bonifacino, J.S. and Glick, B.S. (2004) The mechanisms of vesicle budding and fusion. *Cell*, **116**, 153–166.
2. Fan, J., Hu, Z., Zeng, L., Lu, W., Tang, X., Zhang, J. and Li, T. (2008) Golgi apparatus and neurodegenerative diseases. *Int. J. Dev. Neurosci.*, **26**, 523–534.
3. Gonatas, N.K., Stieber, A., Mourelatos, Z., Chen, Y., Gonatas, J.O., Appel, S.H., Hays, A.P., Hickey, W.F. and Hauw, J.J. (1992) Fragmentation of the Golgi apparatus of motor neurons in amyotrophic lateral sclerosis. *Am. J. Pathol.*, **140**, 731–737.
4. Mourelatos, Z., Gonatas, N.K., Stieber, A., Gurney, M.E. and Dal Canto, M.C. (1996) The Golgi apparatus of spinal cord motor neurons in transgenic mice expressing mutant Cu,Zn superoxide dismutase becomes fragmented in early, preclinical stages of the disease. *Proc. Natl. Acad. Sci. U.S.A.*, **93**, 5472–5477.
5. Thyberg, J. and Moskalewski, S. (1985) Microtubules and the organization of the Golgi complex. *Exp. Cell Res.*, **159**, 1–16.
6. Cole, N.B., Sciaky, N., Marotta, A., Song, J. and Lippincott-Schwartz, J. (1996) Golgi dispersal during microtubule disruption: regeneration of Golgi stacks at peripheral endoplasmic reticulum exit sites. *Mol. Biol. Cell*, **7**, 631–650.
7. Allan, V.J. and Kreis, T.E. (1986) A microtubule-binding protein associated with membranes of the Golgi apparatus. *J. Cell Biol.*, **103**, 2229–2239.
8. Strey, C.W., Spellman, D., Stieber, A., Gonatas, J.O., Wang, X., Lambris, J.D. and Gonatas, N.K. (2004) Dysregulation of stathmin, a microtubule-destabilizing protein, and up-regulation of Hsp25, Hsp27, and the antioxidant peroxiredoxin 6 in a mouse model of familial amyotrophic lateral sclerosis. *Am. J. Pathol.*, **165**, 1701–1718.
9. Urushitani, M., Sik, A., Sakurai, T., Nukina, N., Takahashi, R. and Julien, J.P. (2006) Chromogranin-mediated secretion of mutant superoxide dismutase proteins linked to amyotrophic lateral sclerosis. *Nat. Neurosci.*, **9**, 108–118.
10. Atkin, J.D., Farg, M.A., Soo, K.Y., Walker, A.K., Halloran, M., Turner, B.J., Nagley, P. and Horne, M.K. (2014) Mutant SOD1 inhibits ER-Golgi transport in amyotrophic lateral sclerosis. *J. Neurochem.*, **129**, 190–204.
11. Stieber, A., Gonatas, J.O., Moore, J.S., Bantly, A., Yim, H.S., Yim, M.B. and Gonatas, N.K. (2004) Disruption of the structure of the Golgi apparatus and the function of the secretory pathway by mutants G93A and G85R of Cu, Zn superoxide dismutase (SOD1) of familial amyotrophic lateral sclerosis. *J. Neurol. Sci.*, **219**, 45–53.
12. Sundaramoorthy, V., Walker, A.K., Yerbury, J., Soo, K.Y., Farg, M.A., Hoang, V., Zeineddine, R., Spencer, D. and Atkin, J.D. (2013) Extracellular wildtype and mutant SOD1 induces ER–Golgi pathology characteristic of amyotrophic lateral sclerosis in neuronal cells. *Cell. Mol. Life Sci.*, **70**, 4181–4195.
13. Schmalbruch, H., Jensen, H.S., Bjaerg, M., Kamieniecka, Z. and Kurland, L. (1991) A new mouse mutant with progressive motor neuronopathy. *J. Neuropathol. Exp. Neurol.*, **50**, 192–204.
14. Martin, N., Jaubert, J., Gounon, P., Salido, E., Haase, G., Szatanik, M. and Guenet, J.L. (2002) A missense mutation in Tbce causes progressive motor neuronopathy in mice. *Nat. Genet.*, **32**, 443–447.
15. Bömmel, H., Xie, G., Rossoll, W., Wiese, S., Jablonka, S., Boehm, T. and Sendtner, M. (2002) Missense mutation in the tubulin-specific chaperone E (Tbce) gene in the mouse mutant progressive motor neuronopathy, a model of human motoneuron disease. *J. Cell Biol.*, **159**, 563–569.
16. Tian, G., Huang, Y., Rommelaere, H., Vandekerckhove, J., Ampe, C. and Cowan, N.J. (1996) Pathway leading to correctly folded beta-tubulin. *Cell*, **86**, 287–296.
17. Tian, G., Lewis, S.A., Feierbach, B., Stearns, T., Rommelaere, H., Ampe, C. and Cowan, N.J. (1997) Tubulin subunits exist in an activated conformational state generated and maintained by protein cofactors. *J. Cell Biol.*, **138**, 821–832.
18. Schaefer, M.K., Schmalbruch, H., Buhler, E., Lopez, C., Martin, N., Guenet, J.L. and Haase, G. (2007) Progressive motor neuronopathy: a critical role of the tubulin chaperone TBCE in axonal tubulin routing from the Golgi apparatus. *J. Neurosci.*, **27**, 8779–8789.
19. Parvari, R., Hershkovitz, E., Grossman, N., Gorodischer, R., Loeys, B., Zecic, A., Mortier, G., Gregory, S., Sharony, R., Kambouris, M. *et al.* (2002) Mutation of TBCE causes hypoparathyroidism–retardation–dysmorphism and autosomal recessive Kenny–Caffey syndrome. *Nat. Genet.*, **32**, 448–452.
20. Haase, G., Kennel, P., Pettmann, B., Vigne, E., Akli, S., Revah, F., Schmalbruch, H. and Kahn, A. (1997) Gene therapy of murine motor neuron disease using adenoviral vectors for neurotrophic factors. *Nat. Med.*, **3**, 429–436.
21. Xiang, Y., Seemann, J., Bisel, B., Punthambaker, S. and Wang, Y. (2007) Active ADP-ribosylation factor-1 (ARF1) is required for mitotic Golgi fragmentation. *J. Biol. Chem.*, **282**, 21829–21837.
22. Guo, Y., Punj, V., Sengupta, D. and Linstedt, A.D. (2008) Coat-tether interaction in Golgi organization. *Mol. Biol. Cell*, **19**, 2830–2843.
23. Nakamura, N., Lowe, M., Levine, T.P., Rabouille, C. and Warren, G. (1997) The vesicle docking protein p115 binds GM130, a *cis*-Golgi matrix protein, in a mitotically regulated manner. *Cell*, **89**, 445–455.
24. Razi, M., Chan, E.Y. and Tooze, S.A. (2009) Early endosomes and endosomal coatomer are required for autophagy. *J. Cell Biol.*, **185**, 305–321.
25. Xu, D. and Hay, J.C. (2004) Reconstitution of COPII vesicle fusion to generate a pre-Golgi intermediate compartment. *J. Cell. Biol.*, **167**, 997–1003.
26. Horstmann, H., Ng, C.P., Tang, B.L. and Hong, W. (2002) Ultrastructural characterization of endoplasmic reticulum–Golgi transport containers (EGTC). *J. Cell. Sci.*, **115**, 4263–4273.
27. Styers, M.L., O'Connor, A.K., Grabski, R., Cormet-Boyaka, E. and Sztul, E. (2008) Depletion of beta-COP reveals a role for COP-I in compartmentalization of secretory compartments and in biosynthetic transport of caveolin-1. *Am. J. Physiol. Cell. Physiol.*, **294**, C1485–C1498.
28. Bentley, M., Liang, Y., Mullen, K., Xu, D., Sztul, E. and Hay, J.C. (2006) SNARE status regulates tether recruitment and function in homotypic COPII vesicle fusion. *J. Biol. Chem.*, **281**, 38825–38833.
29. Subramaniam, V.N., Peter, F., Philp, R., Wong, S.H. and Hong, W. (1996) GS28, a 28-kilodalton Golgi SNARE that participates in ER-Golgi transport. *Science*, **272**, 1161–1163.
30. Xu, Y., Wong, S.H., Zhang, T., Subramaniam, V.N. and Hong, W. (1997) GS15, a 15-kilodalton Golgi soluble *N*-ethylmaleimide-sensitive factor attachment protein receptor (SNARE) homologous to rbet1. *J. Biol. Chem.*, **272**, 20162–20166.
31. Ballensiefen, W., Ossipov, D. and Schmitt, H.D. (1998) Recycling of the yeast v-SNARE Sec22p involves COPI-proteins and the ER transmembrane proteins Ufe1p and Sec20p. *J. Cell. Sci.*, **111**, 1507–1520.
32. Rein, U., Andag, U., Duden, R., Schmitt, H.D. and Spang, A. (2002) ARF-GAP-mediated interaction between the ER-Golgi v-SNAREs and the COPI coat. *J. Cell Biol.*, **157**, 395–404.

33. Haase, G., Pettmann, B., Bordet, T., Villa, P., Vigne, E., Schmalbruch, H. and Kahn, A. (1999) Therapeutic benefit of ciliary neurotrophic factor in progressive motor neuronopathy depends on the route of delivery. *Ann. Neurol.*, **45**, 296–304.

34. Stiess, M., Maghelli, N., Kapitein, L.C., Gomis-Ruth, S., Wilsch-Brauninger, M., Hoogenraad, C.C., Tolic-Norrelykke, I.M. and Bradke, F. (2010) Axon extension occurs independently of centrosomal microtubule nucleation. *Science*, **327**, 704–707.

35. Chabin-Brion, K., Marceiller, J., Perez, F., Settegrana, C., Drechou, A., Durand, G. and Pous, C. (2001) The Golgi complex is a microtubule-organizing organelle. *Mol. Biol. Cell*, **12**, 2047–2060.

36. Miller, P.M., Folkmann, A.W., Maia, A.R., Efimova, N., Efimov, A. and Kaverina, I. (2009) Golgi-derived CLASP-dependent microtubules control Golgi organization and polarized trafficking in motile cells. *Nat. Cell Biol.*, **11**, 1069–1080.

37. Skoufias, D.A., Burgess, T.L. and Wilson, L. (1990) Spatial and temporal colocalization of the Golgi apparatus and microtubules rich in detyrosinated tubulin. *J. Cell Biol.*, **111**, 1929–1937.

38. Vainberg, I.E., Lewis, S.A., Rommelaere, H., Ampe, C., Vandekerckhove, J., Klein, H.L. and Cowan, N.J. (1998) Prefoldin, a chaperone that delivers unfolded proteins to cytosolic chaperonin. *Cell*, **93**, 863–873.

39. Gao, Y., Thomas, J.O., Chow, R.L., Lee, G.H. and Cowan, N.J. (1992) A cytoplasmic chaperonin that catalyzes beta-actin folding. *Cell*, **69**, 1043–1050.

40. Tian, G., Bhamidipati, A., Cowan, N.J. and Lewis, S.A. (1999) Tubulin folding cofactors as GTPase-activating proteins. GTP hydrolysis and the assembly of the alpha/beta-tubulin heterodimer. *J. Biol. Chem.*, **274**, 24054–24058.

41. Tian, G., Kong, X.P., Jaglin, X.H., Chelly, J., Keays, D. and Cowan, N.J. (2008) A pachygyria-causing alpha-tubulin mutation results in inefficient cycling with CCT and a deficient interaction with TBCB. *Mol. Biol. Cell*, **19**, 1152–1161.

42. Bhamidipati, A., Lewis, S.A. and Cowan, N.J. (2000) ADP ribosylation factor-like protein 2 (Arl2) regulates the interaction of tubulin-folding cofactor D with native tubulin. *J. Cell Biol.*, **149**, 1087–1096.

43. Watson, P., Forster, R., Palmer, K.J., Pepperkok, R. and Stephens, D.J. (2005) Coupling of ER exit to microtubules through direct interaction of COPII with dynactin. *Nat. Cell Biol.*, **7**, 48–55.

44. Carreno, S., Engqvist-Goldstein, A.E., Zhang, C.X., McDonald, K.L. and Drubin, D.G. (2004) Actin dynamics coupled to clathrin-coated vesicle formation at the trans-Golgi network. *J. Cell Biol.*, **165**, 781–788.

45. Anitei, M., Stange, C., Parshina, I., Baust, T., Schenck, A., Raposo, G., Kirchhausen, T. and Hoflack, B. (2010) Protein complexes containing CYFIP/Sra/PIR121 coordinate Arf1 and Rac1 signalling during clathrin-AP-1-coated carrier biogenesis at the TGN. *Nat. Cell Biol.*, **12**, 330–340.

46. Orci, L., Ravazzola, M., Volchuk, A., Engel, T., Gmachl, M., Amherdt, M., Perrelet, A., Sollner, T.H. and Rothman, J.E. (2000) Anterograde flow of cargo across the Golgi stack potentially mediated via bidirectional 'percolating' COPI vesicles. *Proc. Natl. Acad. Sci. U.S.A.*, **97**, 10400–10405.

47. Sagiv, Y., Legesse-Miller, A., Porat, A. and Elazar, Z. (2000) GATE-16, a membrane transport modulator, interacts with NSF and the Golgi v-SNARE GOS-28. *EMBO J.*, **19**, 1494–1504.

48. Zhong, W., Zhou, Y., Li, S., Zhou, T., Ma, H., Wei, K., Li, H., Olkkonen, V.M. and Yan, D. (2011) OSBP-related protein 7 interacts with GATE-16 and negatively regulates GS28 protein stability. *Exp. Cell Res.*, **317**, 2353–2363.

49. Voloshin, O., Gocheva, Y., Gutnick, M., Movshovich, N., Bakhrat, A., Baranes-Bachar, K., Bar-Zvi, D., Parvari, R., Gheber, L. and Raveh, D. (2010) Tubulin chaperone E binds microtubules and proteasomes and protects against misfolded protein stress. *Cell. Mol. Life Sci.*, **67**, 2025–2038.

50. Xu, X., Kedlaya, R., Higuchi, H., Ikeda, S., Justice, M.J., Setaluri, V. and Ikeda, A. (2010) Mutation in archain 1, a subunit of COPI coatomer complex, causes diluted coat color and Purkinje cell degeneration. *PLoS Genet.*, **6**, e1000956.

51. Blot, S., Poirier, C. and Dreyfus, P.A. (1995) The mouse mutation muscle deficient (mdf) is characterized by a progressive motoneuron disease. *J. Neuropathol. Exp. Neurol.*, **54**, 812–825.

52. Schmidt, W.M., Kraus, C., Hoger, H., Hochmeister, S., Oberndorfer, F., Branka, M., Bingemann, S., Lassmann, H., Muller, M., Macedo-Souza, L.I. *et al.* (2007) Mutation in the Scyl1 gene encoding amino-terminal kinase-like protein causes a recessive form of spinocerebellar neurodegeneration. *EMBO Rep.*, **8**, 691–697.

53. Pelletier, S., Gingras, S., Howell, S., Vogel, P. and Ihle, J.N. (2012) An early onset progressive motor neuron disorder in Scyl1-deficient mice is associated with mislocalization of TDP-43. *J. Neurosci*, **32**, 16560–16573.

54. Jareb, M. and Banker, G. (1997) Inhibition of axonal growth by brefeldin A in hippocampal neurons in culture. *J. Neurosci.*, **17**, 8955–8963.

55. Peter, C.J., Evans, M., Thayanithy, V., Taniguchi-Ishigaki, N., Bach, I., Kolpak, A., Bassell, G.J., Rossoll, W., Lorson, C.L., Bao, Z.Z. *et al.* (2011) The COPI vesicle complex binds and moves with survival motor neuron within axons. *Hum. Mol. Genet.*, **20**, 1701–1711.

56. Ting, C.H., Wen, H.L., Liu, H.C., Hsieh-Li, H.M., Li, H. and Lin-Chao, S. (2012) The spinal muscular atrophy disease protein SMN is linked to the Golgi network. *PLoS One*, **7**, e51826.

57. Custer, S.K., Todd, A.G., Singh, N.N. and Androphy, E.J. (2013) Dilysine motifs in exon 2b of SMN protein mediate binding to the COPI vesicle protein alpha-COP and neurite outgrowth in a cell culture model of spinal muscular atrophy. *Hum. Mol. Genet.*, **22**, 4043–4052.

58. Bi, J., Tsai, N.-P., Lu, H.-Y., Loh, H.H. and Wei, L.-N. (2007) Copb1-facilitated axonal transport and translation of kappa opioid-receptor mRNA. *Proc. Natl. Acad. Sci. U.S.A.*, **104**, 13810–13815.

59. Todd, A.G., Lin, H., Ebert, A.D., Liu, Y. and Androphy, E.J. (2013) COPI transport complexes bind to specific RNAs in neuronal cells. *Hum. Mol. Genet.*, **22**, 729–736.

60. Pun, S., Santos, A.F., Saxena, S., Xu, L. and Caroni, P. (2006) Selective vulnerability and pruning of phasic motoneuron axons in motoneuron disease alleviated by CNTF. *Nat. Neurosci.*, **9**, 408–419.

61. Torres-Benito, L., Neher, M.F., Cano, R., Ruiz, R. and Tabares, L. (2011) SMN requirement for synaptic vesicle, active zone and microtubule postnatal organization in motor nerve terminals. *PLoS One*, **6**, e26164.